Electrochemical and Solid-State Letters, **2** (3) 107-110 (1999)
S1099-0062(98)07-062-1 CCC: $7.00

High Capacity, Temperature-Stable Lithium Aluminum Manganese Oxide Cathodes for Rechargeable Batteries

Yet-Ming Chiang,[*,z] Donald R. Sadoway,[*] Young-Il Jang,[**] Biying Huang,[*] and Haifeng Wang

Department of Materials Science and Engineering, Massachusetts Institute of Technology, Cambridge, Massachusetts 02139, USA

Manganese oxides are of great interest as low cost and environmentally sound intercalation cathodes for rechargeable lithium batteries, but have suffered from limited capacity and instability upon cycling at the moderately high temperatures (50-70°C) encountered in many applications. Here, we show that $Li_xAl_{0.05}Mn_{0.95}O_2$ of both the monoclinic and orthorhombic ordered rock salt structures exhibit stable cycling and high discharge capacities at elevated temperatures, after an initial transient associated with a spinel like phase transformation. In cells utilizing Li anodes tested at 55°C, rechargeable capacities of 150 mAh/g for the orthorhombic and 200 mAh/g for the monoclinic phase and energy densities ~500 Wh/kg were achieved over more than 100 cycles (2.0-4.4 V). At low current densities, charge capacities approached the theoretical limit. The temperature stability and excellent electrochemical performance, combined with nontoxicity and low raw materials cost, make these compounds attractive cathodes for advanced lithium batteries.

Manuscript submitted July 15, 1998; revised manuscript received October 12, 1998. Available electronically January 11, 1999.

Lithium-ion batteries are presently the power source of choice for portable electronics due to their reliability, safety, and high energy density on a volume or weight basis. Commercial applications of batteries based on $LiCoO_2$ intercalation cathodes have undergone enormous growth since 1995, and provided that performance and cost can reach accepted goals, implementation in larger scale applications such as electric vehicles is anticipated. An intensive search for new electrode materials has been driven by the need for higher energy density at lower cost. Lithium manganese spinels have been the focus of many cathode studies,[1-4] in large part due to their low cost and toxicity compared to $LiCoO_2$ and $LiNiO_2$. However, $LiMn_2O_4$ spinel exhibits lower rechargeable capacity than $LiCoO_2$ (115-120 vs. 120-135 mAh/g),[5] and rapid capacity fade at elevated temperatures in the range of 50-70°C.[6-9] Several recent studies have focused on metastable or disordered manganese oxides. Monoclinic $LiMnO_2$ (*m*-$LiMnO_2$) with the layered rock salt structure (α-$NaFeO_2$ type) has been synthesized by ion exchange of lithium salts with $NaMnO_2$[10] and by hydrothermal reaction,[11] but capacity is low and significant fade has been reported in room-temperature tests to date. Orthorhombic $LiMnO_2$ (*o*-$LiMnO_2$) of the ordered rock salt structure described by Hoppe et al.[12] has also been studied by several groups,[13-15] and has been prepared with varying degrees of crystallographic disorder. Increased capacity (initial values at room temperature exceeding 200 mAh/g) is seen in the more disordered forms of this material, but is also accompanied by greater capacity fade.[15] As we show, the cycling performance of *o*-$LiMnO_2$ at elevated temperatures is also poor. Amorphous manganese oxyiodide[16] and manganese oxide[17] cathodes have recently been synthesized, in which high rechargeable capacities (260-278 mAh/g) are achievable upon insertion to lower voltages (< 2 V). The elevated temperature properties of these materials have not been reported.

An attractive cathode material would meet or exceed the electrochemical performance and elevated temperature stability of $LiCoO_2$, while retaining the low cost of the manganese oxides. The aluminum-doped manganese oxides of this work appear to meet this goal. We originally focused on $Li_xAl_yMn_{1-y}O_2$ solid solutions in order to investigate the effect of aluminum doping on intercalation voltage, extending a study in which aluminum doping was found to increase voltage in $LiCoO_2$.[18] *m*-$LiMnO_2$ (*C*2/m) has the same layered cation ordering as $LiCoO_2$ (*R*$\bar{3}$*m* space group, α-$NaFeO_2$ structure type). In a previous paper we showed that $Li_xAl_yMn_{1-y}O_2$ solid solutions can be stabilized in this structure under reducing synthesis conditions.[19] As discussed later, the solid solubility of Al in $LiMnO_2$ is too low for a meaningful test of voltage effects in this system. However, the monoclinic phase of composition $LiAl_{0.25}Mn_{0.75}O_2$ showed discharge capacity as high as 180 mAh/g at room temperature in short term cycling.[19] Here we report on the discovery of an unanticipated attribute of aluminum doping, namely, the improvement of elevated temperature stability and capacity in both the monoclinic and orthorhombic polymorphs of $Li_xAl_yMn_{1-y}O_2$.

Experimental

Compositions $Li_xAl_yMn_{1-y}O_2$ (x = 1.05, y = 0.05, 0.07, and 0.25) were synthesized in the form of fine powders by a coprecipitation and freeze-drying route as previously reported.[19,20] The slight excess of Li was introduced to compensate for losses during firing. The solid solubility of Al, and the relative stability of the monoclinic and orthorhombic phases, were determined through systematic firing experiments in the temperature range 800-1100°C and over ten decades of oxygen activity (P_{O_2} = 10^{-2} to 10^{-12} atm), controlled using Ar/O_2 and CO/CO_2 gas mixtures. Scanning transmission electron microscopy (STEM, Fisons/VG HB603 instrument) was used to measure directly the Al/Mn ratio in individual oxide particles, and STEM imaging and X-ray diffraction (XRD) were used to detect the aluminum-rich phase γ-$LiAlO_2$ (the sole impurity phase formed). The structures of the major manganese oxide phases were identified using XRD and simulations of model structures with commercial software Cerius[2] (v. 3.5, Molecular Simulations Inc., San Diego, CA). In addition to XRD, transmission electron microscopy (TEM) and selected area diffraction (SAD) of individual oxide particles in the cycled cathodes were used to understand the cycling induced phase transformations.

Electrochemical tests were performed using test cells in which the cathode was prepared as a mixture of the oxide powder, carbon black, graphite, and poly(vinylidene fluoride) (weight ratio 78:6:6:10). These mixtures were compacted at 4 t cm^{-2} in pellets 10-25 mg in weight and 0.5 cm^2 in cross-sectional area. In the test cells, these were separated from a Li metal foil anode by a Celgard 2400 membrane, and flooded with 1 M $LiPF_6$ in ethylene carbonate-diethylene carbonate (1:1 volume ratio) liquid electrolyte. Charge-discharge studies were performed with a Maccor series 4000 automated tester at room temperature and at 55°C. Details of cell assembly and testing are published elsewhere.[21]

Results and Discussion

Monoclinic and orthorhombic phase powders were obtained at P_{O_2} < 10^{-4} atm in the temperature range 800-1000°C. Undoped $LiMnO_2$ crystallizes entirely in the orthorhombic phase under these conditions (Fig. 1d), showing that the Mn valence is predominantly 3+. In this temperature range significant reduction to Mn^{2+} (e.g., appearance of MnO) was not detected for P_{O_2} > 10^{-12} atm. The monoclinic phase was stabilized within a narrow window of temperature and oxygen activity for aluminum-doped compositions, but was not obtained under any firing condition in the absence of aluminum doping. A very nearly single-phase monoclinic $Li_xAl_{0.05}Mn_{0.95}O_2$ was obtained after firing at T = 950°C and P_{O_2} = 10^{-7} atm for 2 h (Fig. 1a). XRD was used to distinguish this phase from cubic spinel, which has a similar diffraction pattern, as discussed previously.[19] STEM compositional mapping (Fig. 2)

* Electrochemical Society Active Member.
** Electrochemical Society Student Member.
z E-mail: YCHIANG@MIT.EDU

S1099-0062(98)07-062-1 CCC: $7.00

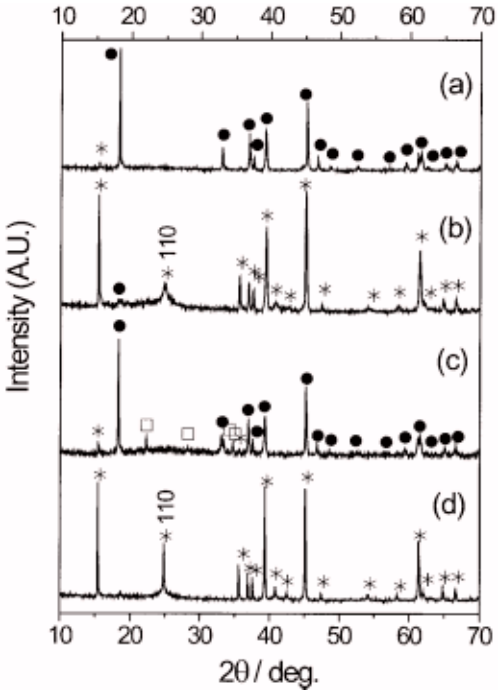

Figure 1. XRD for chemically synthesized $Li_xAl_yMn_{1-y}O_2$ materials showing variation in phase stability with firing temperature and oxygen activity. Results for 2 h firings. ● indicates (*hkl*) lines for the monoclinic phase and ★ indicates those for the orthorhombic phase. (a) *m*-$LiAl_{0.05}Mn_{0.95}O_2$, fired at 950°C, p_{O_2} = 10^{-7} atm. (b) *o*-$LiAl_{0.05}Mn_{0.95}O_2$, fired at 800°C, p_{O_2} = 10^{-12} atm. (c) *m*-$LiAl_{0.25}Mn_{0.75}O_2$, fired at 950°C, p_{O_2} = 10^{-7} atm. (d) *o*-$LiMnO_2$, fired at 950°C, p_{O_2} = 10^{-6} atm. Symbol □ in (c) indicates γ-$LiAlO_2$ (tetragonal).

showed that Al and Mn are uniformly distributed throughout the crystalline oxide particles. Compositions with y = 0.07 and 0.25 showed detectable γ-$LiAlO_2$ as a secondary phase coexisting with *m*-$Li_xAl_{0.05}Mn_{0.95}O_2$ at T = 950-1000°C (Fig. 1c). Thus in this temperature range, the solid solubility of Al in the monoclinic phase is between y = 0.05 and y = 0.07. As either T or p_{O_2} were decreased, the amount of orthorhombic phase increased at the expense of monoclinic phase, showing an apparent two-phase coexistence field separating monoclinic and orthorhombic single-phase fields. At T = 800°C and p_{O_2} = 10^{-10} atm, nearly single-phase *o*-$Li_xAl_{0.05}Mn_{0.95}O_2$ was obtained (Fig. 1b). The aluminum solubility in the orthorhombic phase was nearly identical to that in the monoclinic phase.

These materials are fine in particle size, yet highly ordered, as opposed to the disordered manganese oxides.[15,22] Direct examination by TEM showed that the particle diameter of the orthorhombic phase powders was 0.1-0.2 μm while that of the monoclinic powders was 0.5-0.8 μm. No significant broadening of XRD peaks was observed (Fig. 1), with the exception of the (110) line in the orthorhombic phase, which has been correlated with the planar defect content in this phase.[22] The *o*-$LiMnO_2$ obtained under the present high temperature firing conditions exhibit a narrow (010) diffraction peak (full width at half-maximum < 0.15°) at 2θ = 24.8° (Fig. 1b, 1d), indicating a low defect content. TEM also showed that the as-fired powder particles were largely free of internal defects.

At 55°C, both *m*-$Li_xAl_yMn_{1-y}O_2$ and *o*-$Li_xAl_yMn_{1-y}O_2$ showed a single first-charging plateau near 4 V, followed immediately by development of two voltage steps at ~4 and ~2.9 V, respectively, upon discharging (Fig. 3). In these continuous cycling tests, further cycling resulted in evolution of the voltage profile into two clear plateaus reminiscent of the $Li_xMn_2O_4$ spinels, as discussed later. However, unlike either undoped or doped $LiMn_2O_4$ spinels,[7-9,23] stable cycling is not limited to the 4 V plateau, but is achieved over both voltage plateaus, allowing reversible extraction of a higher lithium fraction from the crystal. After extended cycling (>30 cycles), a particularly flat 2.9 V plateau (Fig. 3 and 4b) was observed, indicating a two-phase region of

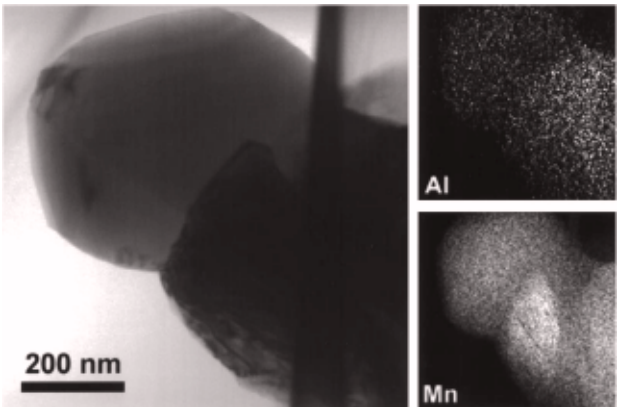

Figure 2. STEM bright-field image and energy-dispersive X-ray composition maps for Al and Mn, showing uniform distribution of the cations.

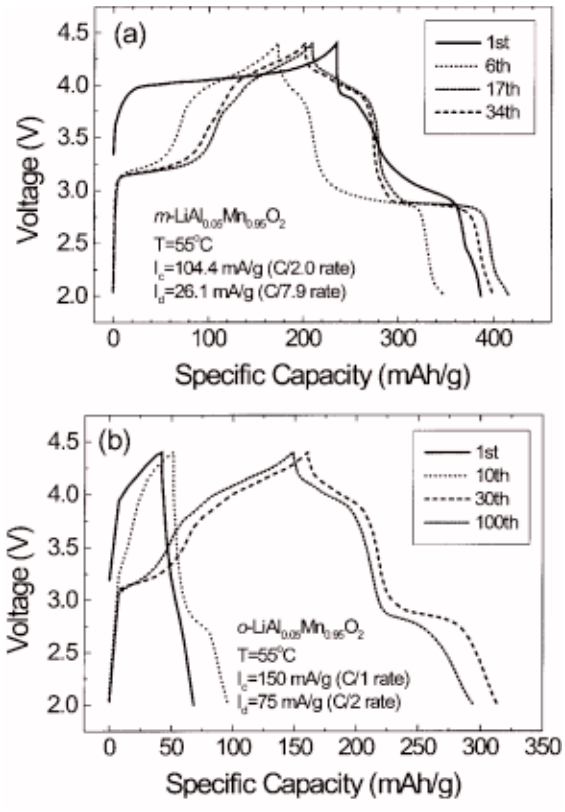

Figure 3. Elevated-temperature cycling tests. (a) Charge/discharge curves at 55°C for a cell containing *m*-$LiAl_{0.05}Mn_{0.95}O_2$ as the cathode. Notice a single plateau during the first charge, followed by evolution to two voltage plateaus at ~4 and ~2.9 V. (b) Charge/discharge curves at 55°C for a cell containing *o*-$LiAl_{0.05}Mn_{0.95}O_2$ as the cathode.

constant Li chemical potential. Consistent with these indications of a cycling-induced structural transformation was a transient capacity response (Fig. 4a), in which the 55°C capacity rises to a peak or steady-state value after 6-30 cycles, depending on the specific material. Similar results were reported for room-temperature tests of *m*-$Li_xAl_yMn_{1-y}O_2$,[19] and were also seen for the *o*-$Li_xAl_yMn_{1-y}O_2$ samples at room temperature (not shown).

Capacity vs. cycling results in Fig. 4 illustrate a central point of this paper: aluminum doping decreases the capacity fade rate of both the monoclinic and orthorhombic polymorphs at elevated temperature. At 55°C, undoped *o*-Li_xMnO_2 loses capacity at a rate

S1099-0062(98)07-062-1 CCC: $7.00

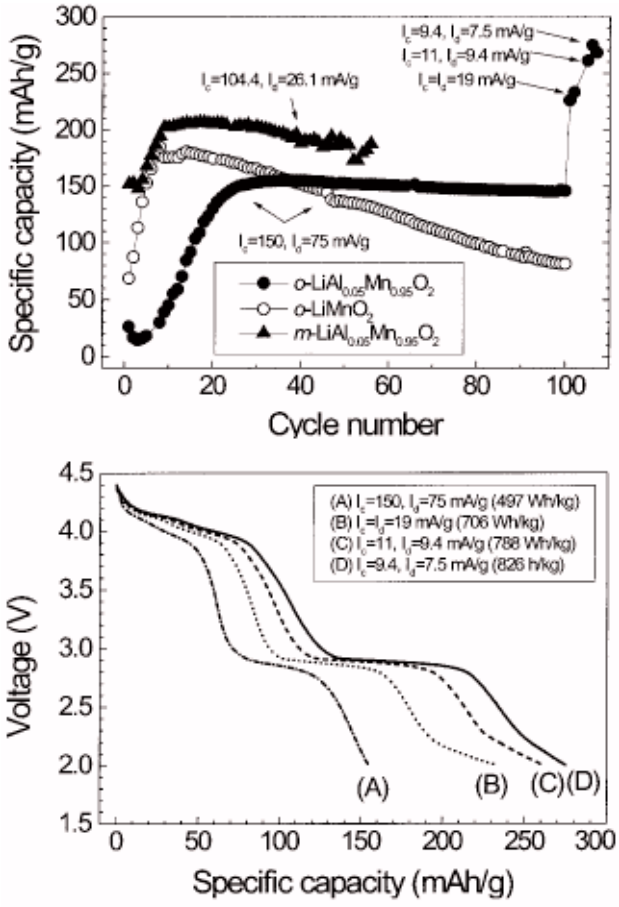

Figure 4. (top) Specific capacity vs. cycle number for monoclinic and orthorhombic polymorphs of $LiAl_{0.05}Mn_{0.95}O_2$, tested at 55°C. Notice lower capacity fade in both aluminum-doped polymorphs. (bottom) Discharge curves for the *o*-$LiAl_{0.05}Mn_{0.95}O_2$, cathode in (a), taken at a lower rate after the 100th cycle. The capacity between 4.4 and 2.0 V approaches the theoretical value of 289 mAh/g based on Mn valence. Note also the flat 2.9 V plateau indicating the coexistence of two phases.

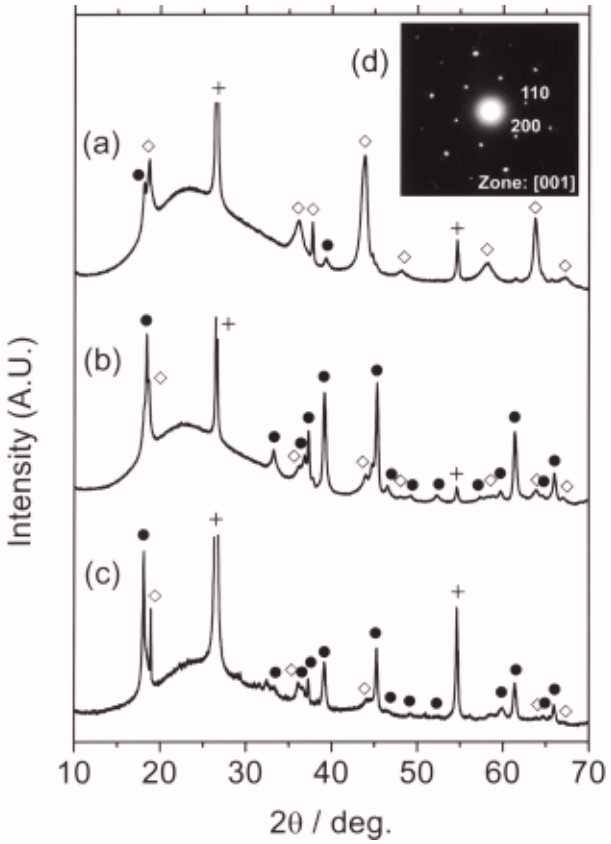

Figure 5. XRD of cycled cathodes examined after discharge to 2.0V. (a) The *o*-$LiMnO_2$ phase has transformed to a predominantly cubic spinel phase (indicated by symbol ◇). (b and c) The monoclinic and orthorhombic phases of $LiAl_{0.05}Mn_{0.95}O_2$ evolve toward similar phase assemblages, consisting of a monoclinic major phase (indicated by symbol ●) and a lesser amount of cubic spinel. Additional minor phases were detected by TEM; see text. (d) SAD pattern from an oxide particle in the *o*-$LiAl_{0.05}Mn_{0.95}O_2$ cathode that has transformed during cycling to the layered monoclinic phase. The reflections and zone axis are indexed in the rhombohedral (α-$NaFeO_2$ structure) setting.

of about 0.5% per cycle, while *m*-$Li_xAl_{0.05}Mn_{0.95}O_2$ and *o*-$Li_xAl_{0.05}Mn_{0.95}O_2$ show loss rates of 0.3[a] and <0.1% per cycle, respectively. As with virtually all intercalation electrodes, the specific values of capacity and energy density were dependent on charge/discharge rate. Figure 4a shows values obtained at charging and discharging rates considered to be realistic for many applications. At 55°C, *m*-$Li_xAl_{0.05}Mn_{0.95}O_2$ and *o*-$Li_xAl_{0.05}Mn_{0.95}O_2$ show discharge capacities of 188 and 146 mAh/g, respectively, after extensive cycling. The corresponding energy densities are 602 and 465 Wh/kg, which are comparable to those for the $LiCoO_2$ and $LiMn_2O_4$ spinel (480-520 Wh/kg).[5] After the initial transient response, the coulombic efficiency exceeded 95% under these test conditions. In contrast, the undoped *o*-Li_xMnO_2 reaches a higher peak capacity of 185 mAh/g, but fades rapidly to 82 mAh/g by 100 cycles (Fig. 4a).

Upon decreasing the charge/discharge rate, the capacities of both phases increased to nearly the theoretical limit for $Li_xAl_{0.05}Mn_{0.95}O_2$.[b] After first cycling the cells 100 times at the above rates, a lower current density was applied, still at 55°C. As shown in Fig. 4a and b, at $I_c = I_d$ = 19 mA/g, discharge capacities of 233 mAh/g and energy densities 706 Wh/kg were obtained in *o*-$Li_xAl_{0.05}Mn_{0.95}O_2$. At I_d = 9.4 and 7.5 mA/g, discharge capacities reached 260-280 mAh/g and energy densities reached 788-826 Wh/kg. Similar tests conducted on *m*-$Li_xAl_{0.05}Mn_{0.95}O_2$ yielded 249 mAh/g (786 Wh/kg). The coulombic efficiency at these lower current densities was essentially 100%. Note in Fig. 4b that additional capacity below the cutoff of 2.0 V appears accessible, suggesting that the aluminum-doped compounds can intercalate lithium even beyond the theoretical limit defined by the manganese valence state.

Although both the starting structure of the compounds and the observation of a single first-charging plateau indicate that lithium is removed from octahedrally coordinated sites during the first charge, all three of the tested materials show an evolution toward two voltage plateaus upon discharge, suggesting a structural transformation to spinel-like cation ordering.[3,14,15,19] The 4 V plateau over which the lithium concentration varies between $0 < x < 1$ is believed to correspond to insertion at 8a tetrahedral sites, while the 3 V plateau over which $1 < x < 2$ corresponds to insertion at 16c octahedral sites as a collective shift of Li ions from 8a to 16c sites occurs at high lithium concentrations.[24] To understand possible structural origins of the unusual stability of the aluminum-doped materials, we conducted XRD and TEM analysis of cycled cathodes in the fully lithiated state (i.e., discharged to 2.0 V). A striking difference was observed between the *m*-$Li_xAl_{0.05}Mn_{0.95}O_2$ and *o*-$Li_xAl_{0.05}Mn_{0.95}O_2$ compositions in comparison to the undoped *o*-$LiMnO_2$.

Addressing first the undoped *o*-$LiMnO_2$, we found by XRD that it indeed shows a transformation to spinel (Fig. 5a), but that in the fully lithiated state this appears to be predominantly a cubic spinel and not the tetragonal spinel that normally results upon lithiation of

[a] This cell showed lithium metal dendrites upon disassembly, suggesting cell degradation may have occurred, in which case the true capacity fade of the oxide may be lower than 0.3% per cycle.

[b] Assuming reversible intercalation between compositions of $x = 0$ and 1, the theoretical capacity is 289.7 mAh/g for the composition $Li_xAl_{0.05}Mn_{0.95}O_2$.

S1099-0062(98)07-062-1 CCC: $7.00

$LiMn_2O_4$.[25] (While the tetragonal spinel XRD is not displayed, the two are readily distinguishable from one another by XRD.) The collective Jahn-Teller distortion that occurs at average Mn valence <3.5+,[26] and to which cycling fade of the spinels has been attributed,[27] has apparently been suppressed. TEM showed that while the cycled *o*-$LiMnO_2$ particles were strained and occasionally fractured, as has been seen in $LiCoO_2$ cathodes,[28] the transformation to cubic spinel did occur uniformly throughout individual particles (as opposed to nucleation of new particles of spinel phase). Suppression of the tetragonal spinel distortion and the associated electromechanical damage may be responsible for the more stable cycling of *o*-$LiMnO_2$ compared to conventional $LiMn_2O_4$ spinel.

Analysis of the cycled *m*-$Li_xAl_{0.05}Mn_{0.95}O_2$ and *o*-$Li_xAl_{0.05}Mn_{0.95}O_2$ cathodes by XRD and TEM revealed a more complex phase assemblage. First, by XRD it was observed that both phases evolve after ~100 cycles at 55°C toward the same phase assemblage (Fig. 5b and c). The cycled cathodes show predominantly two sets of reflections, one of which is the cubic spinel. The second set of reflections, which represents the larger fraction of the oxide total, appears to constitute a mixture of the monoclinic phase and the tetragonal spinel. In a previous paper,[19] we examined the distinctions between the tetragonal and monoclinic phases in XRD data using computer simulations of various assumed structures, and showed that while the two have very similar XRD patterns, they are distinguishable from one another by the relative intensities and positions of diffraction peaks in the $2\theta = 65\text{-}68°$ range (using Cu Kα radiation; Fig. 2 in Ref. 19). Careful scrutiny of these XRD peaks for both aluminum-doped cathodes after cycling indicates the presence of both monoclinic and tetragonal phases. SAD of individual cycled oxide particles using TEM also showed the presence of multiple phases, although spinel is a major phase. In the cycled *m*-$Li_xAl_{0.05}Mn_{0.95}O_2$ cathode, monoclinic phase and cubic-spinel particles were observed, along with a yet-unidentified phase. In the cycled *o*-$Li_xAl_{0.05}Mn_{0.95}O_2$ cathode, the monoclinic and cubic spinel phases, some residual orthorhombic phase, one instance of a tetragonal spinel particle, and the same unidentified phase were seen. A recent study of cycled $LiCoO_2$ cathodes[28] has shown that electrochemically induced damage and cation disorder occur nonuniformly within a composite cathode. In the present materials, even though the starting materials are single phase, it is not surprising that there is some variation in the cycling-induced phase transformations from particle to particle, as the rate and depth of charge/discharge are likely to vary at the particle level.

The apparent transformation of the orthorhombic phase during cycling is particularly surprising. Figure 5d shows the SAD pattern from a particle in the cycled *o*-$Li_xAl_{0.05}Mn_{0.95}O_2$ cathode, showing six-fold symmetry. Simulations have been conducted of the SAD patterns of $LiMO_2$ and LiM_2O_4 oxides (where M is the metal) of several ideally ordered and partially disordered structures.[28] The α-$NaFeO_2$ structure type, cubic LiM_2O_4 spinel, and so-called lithiated spinel $Li_2M_2O_4$ in which Li occupies 16c octahedral sites have all been simulated, and of these, the SAD pattern in Fig. 5d can be explained only by layered α-$NaFeO_2$ type ordering. Unlike the cycled *m*-$Li_xAl_{0.05}Mn_{0.95}O_2$, in which detection of the monoclinic phase could simply indicate some untransformed starting material, the appearance of the monoclinic phase in cycled *o*-$Li_xAl_{0.05}Mn_{0.95}O_2$ is evidence for a cycling-induced transformation. This in turn suggests that the monoclinic phase of $LiMnO_2$ is stabilized by aluminum doping. As was previously seen under high temperature synthesis conditions.[19]

The very flat 2.9 V discharge plateau in the cycled cathodes (Fig. 4) indicates a constant lithium chemical potential in the cathode that requires the coexistence of at least two phases, assuming local equilibrium. The cycled cathodes certainly satisfy this requirement. The near-theoretical values of discharge capacity further indicate that the oxide is nearly completely delithiated and lithiated during cycling. A more specific interpretation of the voltage-capacity profile, in the context of the phases present, requires more detailed knowledge of the phase fractions and the intercalation behavior of each phase. Both the spinel and monoclinic polymorphs can contribute capacity on the 4 V plateau, while presumably only the spinel phase(s) provide capacity on the 2.9 V plateau. Since we have only examined the phase assemblage in the fully discharged state, it is also possible that a more complex sequence of phase changes takes place during intercalation. More detailed examination of the evolution of phases as a function of cycle number and at different states of charge/discharge seems warranted, and is underway.

Conclusions

Compounds of composition $Li_xAl_yMn_{1-y}O_2$ can be crystallized in either the monoclinic derivative of the α-$NaFeO_2$ structure type or the orthorhombic ordered rock salt structure, depending on the temperature and oxygen activity imposed during high temperature synthesis. Undoped $LiMnO_2$ crystallizes only in the orthorhombic phase under the same conditions. Both aluminum-doped polymorphs appear to be promising cathode materials for advanced lithium batteries, as they exhibit much improved resistance to cycling fade at 55°C compared to undoped *o*-$LiMnO_2$ or a $LiMn_2O_4$ spinel, possess high charge capacities in some instances approaching the theoretical limit (289 mAh/g), and can be made from low cost raw materials. While both the monoclinic and orthorhombic phases exhibit a cycling-induced change in the voltage profile, unlike the $LiMn_2O_4$ spinel, the capacity is stable upon cycling over both the 4 and 3 V plateaus. In undoped *o*-$LiMnO_2$, this stability is attributed to a cycling-induced transformation to a stable cubic spinel phase, while in both of the aluminum-doped polymorphs, evolution to a more complex multiphase mixture is observed.

Acknowledgments

This work was supported by the INEEL University Research Consortium, managed by Lockheed Martin Idaho Technology Company for the U.S. Department of Energy, Idaho Operations Offices, under contract no. DE-AC07-94ID13223. Instrumentation in the Shared Central Facilities at MIT, supported by NSF grant no. 9400334-DMR, was used. Y.I.J. also acknowledges a fellowship from the Ministry of Education, Korea.

The Massachusetts Institute of Technology assisted in meeting the publication costs of this article.

References

1. T. Ohzuku, M. Kitagawa, and T. Hirai, *J. Electrochem. Soc.*, **137**, 769 (1990).
2. J. M. Tarascon, E. Wang, F. K. Shokoohi, W. R. McKinnon, and S. Colson, *J. Electrochem. Soc.*, **138**, 2859 (1991).
3. R. J. Gummow, A. de Kock, and M. M. Thackeray, *Solid State Ionics*, **69**, 59 (1994).
4. Y. Gao and J. R. Dahn, *J. Electrochem. Soc.*, **143**, 100 (1996).
5. R. Koksbang, J. Barker, H. Shi, and M. Y. Saïdi, *Solid State Ionics*, **84**, 1 (1996).
6. Y. Xia, Y. Zhou, and M. Yoshio, *J. Electrochem. Soc.*, **144**, 2593 (1997).
7. G. G. Amatucci, C. N. Schmutz, A. Blyr, C. Sigala, A. S. Gozdz, D. Larcher, and J. M. Tarascon, *J. Power Sources*, **69**, 11 (1997).
8. G. G. Amatucci, A. Blyr, C. Sigala, P. Alfonse, and J. M. Tarascon, *Solid State Ionics*, **104**, 13 (1997).
9. A. Blyr, C. Sigala, G. G. Amatucci, D. Guyomard, Y. Chabre, and J. M. Tarascon, *J. Electrochem. Soc.*, **145**, 194 (1998).
10. A. R. Armstrong and P. G. Bruce, *Nature*, **381**, 499 (1996).
11. M. Tabuchi, K. Ado, H. Kobayashi, H. Kageyama, C. Masqulier, A. Kondo, and R. Kanno, *J. Electrochem. Soc.*, **145**, L49 (1998).
12. R. Hoppe, G. Brachtel, and M. Jansen, *Z. Anorg. Allg. Chem.*, **417**, 1 (1975).
13. T. Ohzuku, A. Ueda, and T. Harai, *Chem. Express*, **7**, 193 (1992).
14. J. N. Reimers, E. W. Fuller, E. Rossen, and J. R. Dahn, *J. Electrochem. Soc.*, **140**, 3396 (1993).
15. L. Croguennec, P. Deniard, and R. Brec, *J. Electrochem. Soc.*, **144**, 3323 (1997).
16. J. Kim and A. Manthiram, *Nature*, **390**, 265 (1997).
17. J. J. Xu, A. J. Kinser, B. B. Owens, and W. H. Smyrl, *Electrochem. Solid-State Lett.*, **1**, 1 (1998).
18. G. Ceder, Y.-M. Chiang, D. R. Sadoway, M. K. Aydinol, Y.-I. Jang, and B. Huang, *Nature*, **392**, 694 (1998).
19. Y.-I. Jang, B. Huang, Y.-M. Chiang, and D. R. Sadoway, *Electrochem. Solid-State Lett.*, **1**, 13 (1998).
20. Y.-M. Chiang, Y.-I. Jang, H. Wang, B. Huang, D. R. Sadoway, and P. Ye, *J. Electrochem. Soc.*, **145**, 887 (1998).
21. B. Huang, Y.-I. Jang, Y.-M. Chiang, and D. R. Sadoway, *J. Appl. Electrochem.*, In press.
22. L. Croguennec, P. Deniard, R. Brec, and A. Lecerf, *J. Mater. Chem.*, **7**, 511 (1997).
23. A. D. Robertson, S. H. Lu, and W. F. Howard, Jr., *J. Electrochem. Soc.*, **144**, 3505 (1997).
24. M. M. Thackeray, W. I. F. David, P. G. Bruce, and J. B. Goodenough, *Mater. Res. Bull.*, **18**, 461 (1983).
25. J. M. Tarascon and D. Guyomard, *J. Electrochem. Soc.*, **138**, 2864 (1991).
26. M. M. Thackeray, A de Kock, M. H. Rossouw, D. Liles, R. Bittihn, and D. Hoge, *J. Electrochem. Soc.*, **139**, 363 (1992).
27. J. Barker, R. Koksbang, and M. Y. Saïdi, *Solid State Ionics*, **82**, 143 (1995).
28. H. Wang, Y.-I. Jang, B. Huang, D. R. Sadoway, and Y.-M. Chiang, *J. Electrochem. Soc.*, To be published.